GEOPHYSICS, VOL. 72, NO. 1 (JANUARY-FEBRUARY 2007); P. P9–P21, 19 FIGS.
10.1190/1.2392789

Unsupervised seismic facies analysis using wavelet transform and self-organizing maps

Marcílio Castro de Matos[1], Paulo Léo Manassi Osorio[2], and Paulo Roberto Schroeder Johann[3]

ABSTRACT

Unsupervised seismic facies analysis provides an effective way to estimate reservoir properties by combining different seismic attributes through pattern recognition algorithms. However, without consistent geological information, parameters such as the number of facies and even the input seismic attributes are usually chosen in an empirical way. In this context, we propose two new semiautomatic alternative methods. In the first one, we use the clustering of the Kohonen self-organizing maps (SOMs) as a new way to build seismic facies maps and to estimate the number of seismic facies. In the second method, we use wavelet transforms to identify seismic trace singularities in each geologically oriented segment, and then we build the seismic facies map using the clustering of the SOM. We tested both methods using synthetic and real seismic data from the Namorado deepwater giant oilfield in Campos Basin, offshore Brazil. The results confirm that we can estimate the appropriate number of seismic facies through the clustering of the SOM. We also showed that we can improve the seismic facies analysis by using trace singularities detected by the wavelet transform technique. This workflow presents the advantage of being less sensitive to horizon interpretation errors, thus resulting in an improved seismic facies analysis.

INTRODUCTION

Reservoir models are initially generated from estimates of specific rock properties and maps of reservoir heterogeneity. Estimates of rock properties, including porosity, permeability, fluid type, and lithology, as well as reservoir compartmentalization and thickness, are fundamental for the exploration, development, and production of petroleum fields. Small quantitative errors in the properties, as well as in the reservoir dimensions, can have great economic consequences.

Many types of information are used in reservoir model construction. One of the most important sources of information comes from wells, including well logs, core samples, and production data. However, well log and core data are local measurements that may not reflect the reservoir behavior as a whole. In addition, well data are not available at the initial phases of exploration. Models built using well data require interpolation and extrapolation of local properties measured in the wells to the entire prospect.

In contrast to sparse well data, 3D seismic data cover large areas. Changes in the lithology and fluids result in changes in amplitude, shape, lateral coherence, and other seismic attributes. Seismic attributes can provide information for the construction of reservoir models. The description and interpretation of extracted seismic reflection parameters, which include geometry, continuity, amplitude, frequency, and interval velocity, is known as seismic facies analysis (Mitchum, 1977).

Seismic facies analysis can be accomplished through the use of pattern recognition techniques. Given the appropriate combination of seismic attributes, one can identify lateral changes in the reservoir, which can then be calibrated with well information. The search for an appropriate representation of petroleum reservoirs, using seismic data and pattern recognition techniques, has been the subject of several scientific publications (Dumay and Fournier, 1988; Schultz et al., 1994; Fournier and Derain, 1995; Walls et al., 1999; Johann et al., 2001; Saggaf et al., 2003).

When the geological information is incomplete or nonexistent, seismic facies analysis is called nonsupervised and is performed through unsupervised learning or clustering algorithms (Duda et al.,

Manuscript received by the Editor February 28, 2005; revised manuscript received June 9, 2006; published online December 13, 2006.
[1]Brazilian Army, Military Institute of Engineering and Pontifícia Universidade Católica do Rio de Janeiro, Rua Rangel, 140-Pita, São Gonçalo, Rio de Janeiro, Brazil 24.412-155. E-mail: marciliomatos@gmail.com.
[2]Deceased
[3]Petrobras S. A.-Exploration and Production Department, Av. República do Chile, 65/1704B-Centro, Rio de Janeiro, Brazil 20035-900. E-mail: johann@petrobras.com.br.

2001). One of the most promising mathematical techniques applied to nonsupervised pattern classification is the Kohonen self-organizing map (SOM) (Kohonen, 2001) used by Coléou et al. (2003), Taner et al. (2001), Zhang et al. (2001), and Matos et al. (2003a, b, 2004a, b).

Commercial implementations of the SOM are routinely used to perform seismic facies analysis. However, tasks such as the identification of the number of seismic facies in the analyzed data are still performed in an empirical way.

Regardless of the methodology for seismic facies analysis, the temporal and spatial segmentation of the reservoir area needs to be done carefully. The confidence in the interpretation depends on the geological system complexity, the seismic data quality, and the interpreter's experience (Rankey and Mitchell, 2003), especially because the seismic facies analysis is sensitive to picking errors when using seismic-trace waveforms in the reservoir area.

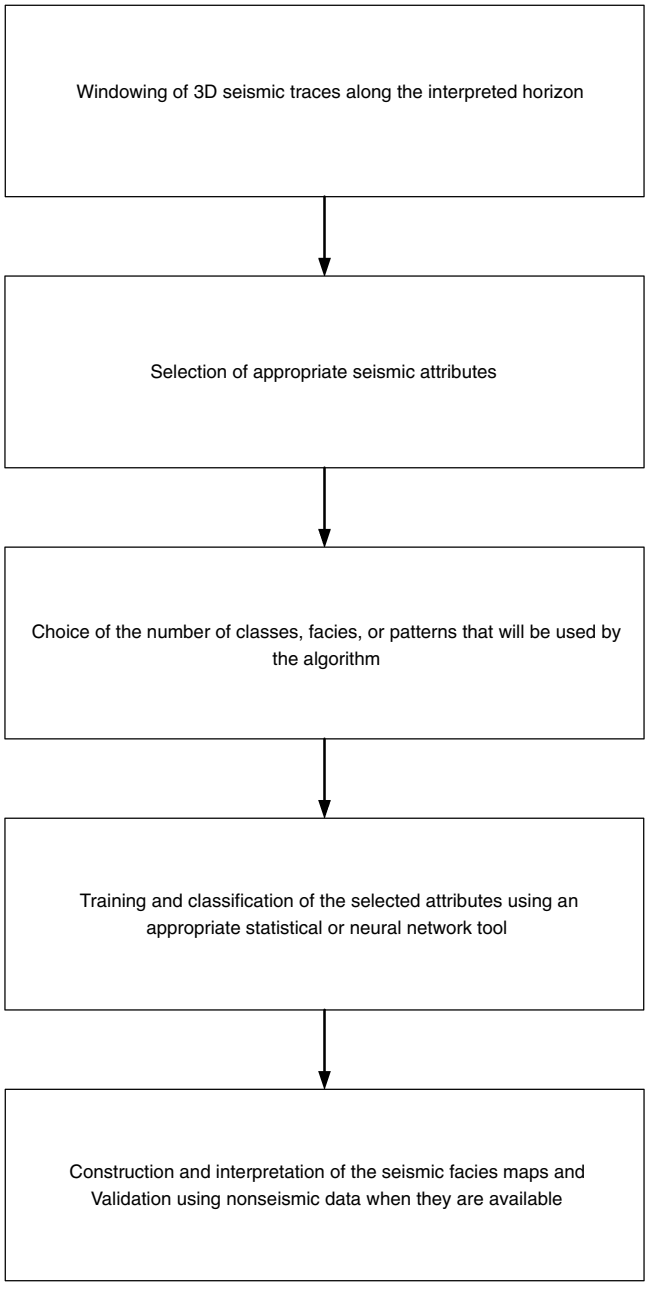

Figure 1. Workflow for seismic facies analysis (Johann et al., 2001).

In this paper, we first review some modern seismic facies analysis techniques. Then, we introduce the concept of the SOM, and we propose the first method that uses the clustering of the SOM, based on the trace waveform, as a new way not only to estimate the number of seismic facies but also as a nonsupervised seismic facies analysis technique (Matos et al., 2003b). Next, we use joint time-frequency analysis to characterize reservoirs because variations in frequency content are sensitive to subtle changes in reflective information (Steeghs and Drijkoningen, 2001). In this context, we show that the continuous wavelet transforms (CWTs) and the discrete wavelet transform (DWT) without time decimation can be applied to detect singularities (Shensa, 1992). We use the concepts of wavelet transform modulus maxima (WTMM); the lines that link the WTMMs are called wavelet transform modulus maxima lines (WTMMLs). Then, we perform the analysis along the WTMML amplitudes, which is called wavelet transform modulus maxima line amplitude (WTMMLA), to characterize the seismic trace singularities. We also propose a second method that uses joint time-frequency properties, obtained through the detection of singularities using wavelet transforms (Matos et al., 2003a, b), as a tool for the detection and characterization of seismic events. These singularities are subject to analysis and SOM clustering. Finally, we tested these two algorithms on synthetic and real data with and without Gaussian noise and seismic interpretation errors.

SOM CLUSTERING ANALYSIS

One of the most important goals of seismic stratigraphy is to recognize and analyze seismic facies with regard to the geologic environment (Dumay and Fournier, 1988). For Sheriff (2002), seismic facies analysis is done by examining seismic traces to identify the characteristics of a group of reflections involving amplitudes, abundance, continuity, and configuration of reflections and also to predict the stratigraphy and depositional environment.

Independent of whether seismic facies analysis is supervised or not, it can be implemented using the workflow shown in Figure 1 (Johann et al., 2001). In spite of its proven effectiveness, the process described above should be performed very carefully.

The SOM (Kohonen, 2001) is currently one of the most important tools for the nonsupervised seismic facies analysis (Coléou et al., 2003).

Kohonen SOMs

An SOM clusters similar data in a manner that provides effective visualization of multidimensional data. An SOM converts statistical relationships among multidimensional data into simple, typically 2D, geometric relationships of the corresponding points. Mathematically, the SOM preserves the metric relationships and the topologies of the multidimensional input in the output 2D net. This net can be used as a visualization tool to show the different data characteristics, with the possibility of group structuring (Taner et al., 2001).

The SOM is closely related to vector quantization methods (Haykin, 1999). We begin by assuming that the input variables, i.e., the seismic attributes, can be represented by vectors in the space $\mathcal{R}^n$, $x = [x_1, x_2, \ldots, x_n]$. The objective of the algorithm is to organize the data set of input seismic attributes delineated by a geometric structure called the SOM. Each SOM unit, defined as a vector prototype, is connected to its neighbors, which in 2D usually forms hexagonal or rectangular structural maps.

We assume that the map has P elements; therefore, there will exist P prototype vectors m_i, $m_i = [m_{i1}, \ldots, m_{in}]$, $i = 1,2,\ldots,P$, where n is the dimension of the input vector, i.e., the number of input seismic attributes. After SOM training, the prototype vectors represent the input data set of seismic attributes.

The number of prototype vectors in the map determines its effectiveness and generalization capacity. During the training, the SOM forms an elastic net that adapts to the cloud formed by the input seismic-attributes data. Data that are close to each other in the input space will also be close to each other in the output map. Because the SOM can be interpreted as a mapping of the input n-dimensional space into a 2D grid that preserves the original topological structure, and because seismic data measures the changes in geology, SOM preserves the topological relation of the underlying geology.

Usually, the SOM prototype vectors are updated iteratively. First, the prototype vectors can either be randomly initialized or initialized by using the projections in the two largest eigenvectors of the input data. Second, for each learning step, an input vector $\boldsymbol{x}$ is randomly chosen from the input data set. The distances between $\boldsymbol{x}$ and all the prototype vectors are computed. The map unit with the smallest distance $\boldsymbol{m}_b$ to the input vector $\boldsymbol{x}$ is called the best matching unit (BMU) and is computed by (Kohonen, 2001)

$$\|x - m_b\| = \min_i\{\|x - m_i\|\}. \qquad (1)$$

Next, the prototype vector corresponding to the BMU and their neighbors are updated, which means that they are moved towards the input winner vector in the input space. The updating rule for the ith unit is given by

$$m_i(t+1) = m_i(t) + \lambda(t)h_{bi}(t)[x - m_i(t)], \qquad (2)$$

where t denotes the iteration, $\lambda(t)$ is the learning rate, and $h_{bi}(t)$ is the neighborhood size centered at the winner unit. The value of $h_{bi}(t)$ decreases with each iteration in the learning process and is given by

$$h_{bi}(t) = e^{-(\|r_b - r_i\|^2/2\sigma^2(t))}, \qquad (3)$$

where r_b and r_i are the positions of the prototype vectors **b** and **i** in the SOM grid and $\sigma^2(t)$ defines the neighborhood width.

Figure 2 shows a very simple example with dimensionless data using the SOM. The input data are the 3D coordinates for three Gaussian-distribution functions, with their centers slightly shifted from each other. There are 3000 3D input vectors corresponding to 3000 measurements of the x-, y-, and z-components. We follow Vesanto and Alhoniemi (2000) to define the 2D map dimensions using the ratio between the two largest eigenvectors of the input data covariance matrix and obtain a 13×7 hexagonal structure giving rise to 91 prototype vectors (Figure 2).

After each iteration of the algorithm, the prototype winner vector and its neighbors are updated using equations 2 and 3. After the learning, the prototype vectors represent not only a means of mapping the input data in the SOM but also a good approximation to the input vectors (Figure 2). Owing to the simplicity of this example, it is very easy to visualize the prototype vectors. Because the number of attributes is often larger than three, the visualization in the input space is usually difficult for general cases. To avoid this limitation, we could project the vector prototypes onto the two or three eigenvectors which correspond to the two or three eigenvalues in the set (Kohonen, 2001).

Because one of the main objectives of this work is the identification of data clusters, we will display the distances between the neighbor prototype vectors to identify similarities among the SOM vector prototypes. Specifically, we will use the unified matrix of distance, or U-matrix (Ultsch, 1993), to represent these distances.

After the SOM learning, the U-matrix is generated by computing, for each SOM prototype vector, the distance between the neighbor prototype vectors and their average. For the prototype vector 33 on the SOM map shown in Figure 3a, we compute the distances to each neighbor (prototype vectors 25, 26, 32, 34, 39, and 40) as well as the average of these distances. In the U-matrix image, the intensity of each pixel corresponds to the respective estimated distance. Therefore, the U-matrix not only shows the average distance between each element, it also shows the gradient between them. Figure 3b shows the U-matrix for the example in Figure 2 in which red or yellow rep-

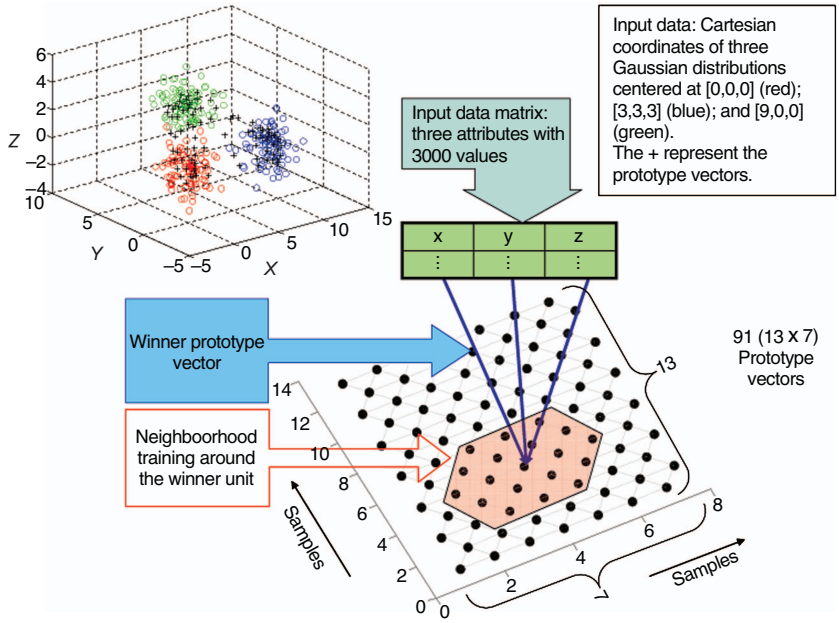

Figure 2. SOM application example showing a map with 91 (13×7) prototype vectors using the coordinates of three Gaussian distributions in 3D space as input attributes.

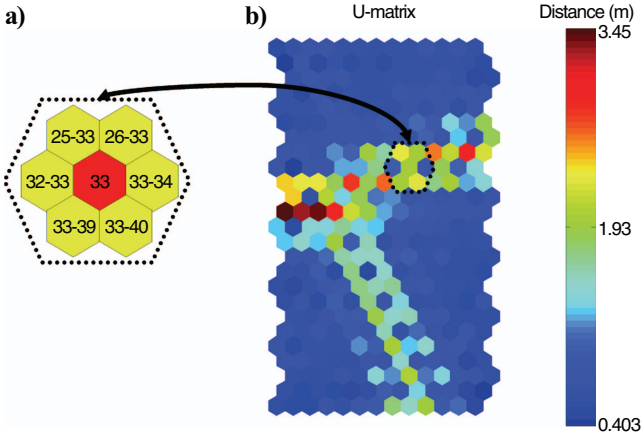

Figure 3. (a) U-matrix generation; (b) U-matrix for the example in Figure 2. Color bar is the distance between the prototype vectors.

resent the prototype vectors that are far apart, whereas blue represents prototype vectors that are close to each other. This 2D topologic image can be visualized as three dense blue valleys which are separated by red, green, and yellow ridges; in other words, they form three outstanding clusters. The U-matrix allows us to visualize the geometry and the number of existing groups in the data. One significant advantage of the SOM is the use of similar colors to map similar classes.

Clustering of the SOM

In nonsupervised seismic facies analysis, the estimation of the number of existing seismic facies in the data is typically determined in an empirical way (Johann et al., 2001).

We propose to estimate the number of seismic facies through SOM visualization. We begin by choosing a number for the SOM prototype vectors that is larger than the number of expected groups in the data. Even though only qualitative information is generated, by using concepts of geomorphology, this procedure can be a quite powerful interpretation tool.

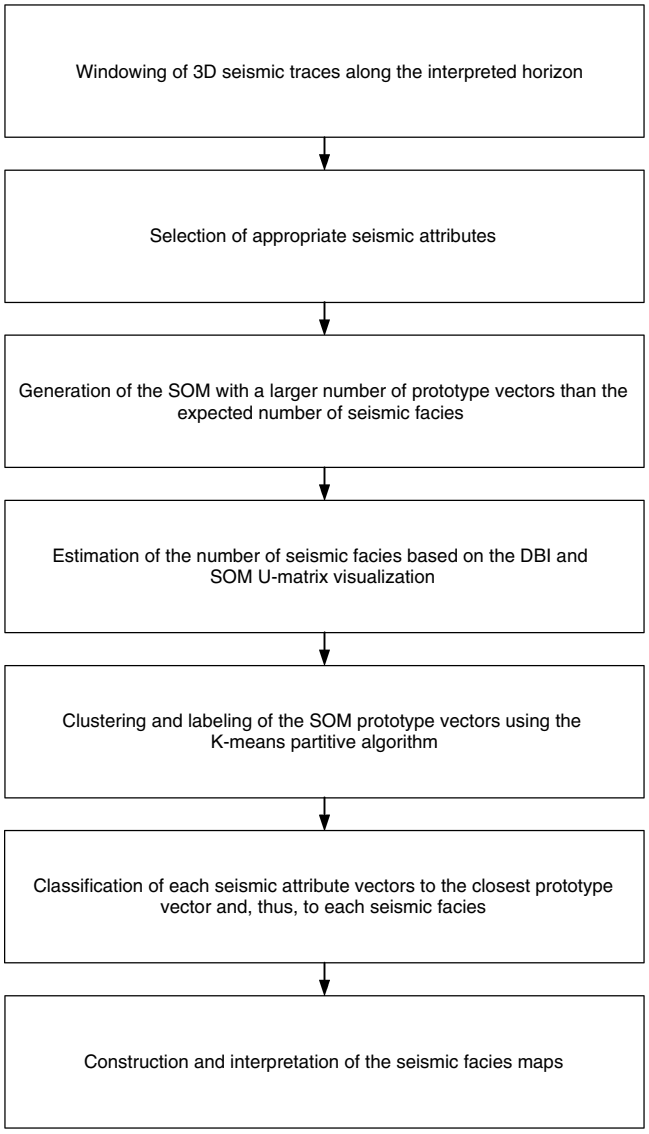

Figure 4. Workflow for nonsupervised seismic facies analysis based on SOM clustering using waveform attributes (first method).

To obtain a more quantitative clustering of data properties, SOM groups could be visualized using the U-matrix and chosen manually. However, the manual selection of the clusters could be tedious and imprecise. Agglomerative, or partitive, SOM clustering or U-matrix segmentation using image processing algorithms (Costa and Netto, 1999) provides an automated means of clustering. We will use a K-means partitive clustering algorithm. In contrast to conventional K-means, we will cluster the prototype vectors instead of the original data (Vesanto and Alhoniemi, 2000). In this manner, large data sets formed by the SOM prototype vectors can be indirectly grouped. The proposed method not only provides a better understanding about the group formations, but it is also computationally efficient (Vesanto et al., 1999). Another benefit of this methodology is noise reduction because the prototype vectors represent local averages of the original data without any loss of resolution.

The K-means clustering

An optimal clustering algorithm should minimize the distance between the elements of each group and, at the same time, maximize the distance between the different clusters. There are several ways of measuring distance (Theodoridis and Koutroumbras, 1999); for simplicity, we will use the Euclidian norm. To compute the distance between the elements of each group, we use the average distance S_k between each element x_i and its group centroid c_k:

$$S_k = \frac{\sum_i \|x_i - c_k\|}{N_k}, \tag{4}$$

where N_k is the number of elements in the group. The distance between the k and l groups is computed as the distance between their centroids:

$$d_{kl} = \|c_k - c_l\|. \tag{5}$$

The partitive clustering algorithm divides the data set into a predefined number of clusters, trying to minimize some error function (Pandya and Macy, 1995, chapter 8), with the number of groups chosen and verified through SOM visualization. To automate the classification process, we use the Davies and Bouldin (1979) index (DBI) as a means of evaluating the results of the K-means partitioning. The best clustering corresponds to the minimum DBI given by

$$\mathrm{DBI} = \frac{1}{K}\sum_{k=1}^{K} \max_{l \neq k}\left\{\frac{S_k + S_l}{d_{kl}}\right\}, \tag{6}$$

where K is the number of groups, S_k and S_l are defined by equation 4, and d_{kl} is defined by equation 5. DBI values smaller than unity represent separate groups, whereas values larger than unity represent groups that may overlap.

SOM CLUSTERING APPLIED TO SEISMIC FACIES ANALYSIS

Principles of the methodology — Seismic facies with the SOM

The flowchart in Figure 4 shows the proposed methodology for nonsupervised seismic facies analysis based on the SOM clustering. The main contribution of this methodology is to assist in the choice of the number of seismic facies in a semiautomatic way.

Seismic facies analysis of synthetic data — Turbidite system model

To verify the effectiveness of the proposed procedure, we used the model shown in Figure 5a (Santos, 1997) to generate the convolutional synthetic cube shown in Figure 5b. The reservoir is represented by three different seismic facies characterized by the their P-wave propagation velocities of 3100 m/s, 3200 m/s, and 3300 m/s.

We used, as seismic attributes (Taner et al., 1994), the seismic amplitudes within a 20-sample window around the reservoir base, i.e., the marked area between blue dotted lines in Figure 6a. The use of the contiguous seismic trace amplitudes as input attributes is equivalent to a waveform classification in the area of interest. The analysis results with the proposed algorithm are shown in Figure 6. Figures 6b–d show the U-matrix, the DBI, and the resulting facies map, respectively. In this example, three groups or facies are easily identified from the U-matrix, and the classification result was excellent. However, the minimum DBI of 4 did not correspond to the number of existing facies. Therefore, the choice of the number of facies should, whenever possible, be done in a semiautomatic way; in other words, the estimate of the facies number should be confirmed by the U-matrix visualization.

This analysis was repeated by adding Gaussian noise to the synthetic seismic model. The result in Figure 7 confirms the good performance obtained with the proposed methodology and reaffirms the importance of the U-matrix visualization for the estimation of the number of seismic facies.

However, when simulating a noisy horizon interpretation in the area of the reservoir, the proposed methodology gave a bad result, as shown in Figure 8. Such a result is related to the chosen seismic attribute, which is known to be sensitive to time displacements (Rankey and Mitchel, 2003). Therefore, the choice of the seismic attributes for the classification of seismic patterns is fundamental to obtain coherent results (Poupon et al., 2004).

Seismic facies analysis of real data — Namorado field, Campos Basin

We now apply the proposed methodology for seismic facies analysis to a 3D seismic real data set from the Campos Basin that was made available by the Brazilian National Petroleum Agency (ANP) and Petrobras. Figure 9 illustrates a dip line and the interpreted reservoir top and base. Nine samples of the reservoir's upper stratigraphic unit (Johann, 1997) were used as an input attribute. Because the variation in reservoir thickness is quite large, nine samples were interpolated inside this stratigraphic unit to avoid the use of samples outside of the interest area. The seismic facies analysis is illustrated in Figure 10. The results show that it is not possible to distinguish any well-defined groups through the U-matrix visualization. It seems that there is a single group with small possible divisions, which means that a clear division doesn't exist among the preponderant trace waveforms in the data. The minimum DBI in Figure 10b indicates the existence of six seismic facies, which is acceptable but not totally justifiable. It is known from the petrophysics analysis of these data that the most probable number of facies is four (Johann, 1997). The maps with four and six facies are shown in Figures 10c and d, respectively.

Thus, the number of seismic facies can not always be identified clearly through SOM clustering. In this case, the choice of seismic-trace amplitudes was inappropriate for seismic facies identification. Geologically, we expect a wide range of waveform variations in the area of interest because the seismic data were extracted from a complex sandstone turbidite system. To address this difficulty, we developed a second method based on time-frequency techniques to locate and emphasize reservoir characteristics.

DETECTION AND CHARACTERIZATION OF SINGULARITIES USING TIME-FREQUENCY TECHNIQUES

Seismic signals are a low-frequency representation of the subsurface reflectivity. Specifically, seismic signals measure changes in

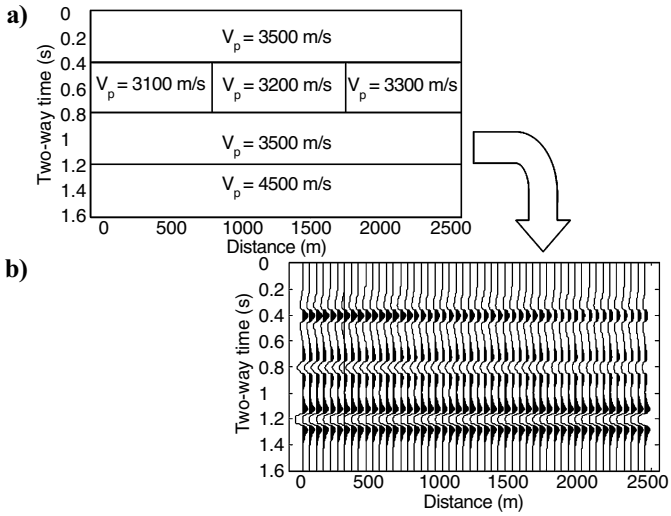

Figure 5. (a) Schematic model with the propagation velocity of each layer; (b) seismic signal synthesized from the velocity model (Santos, 1997).

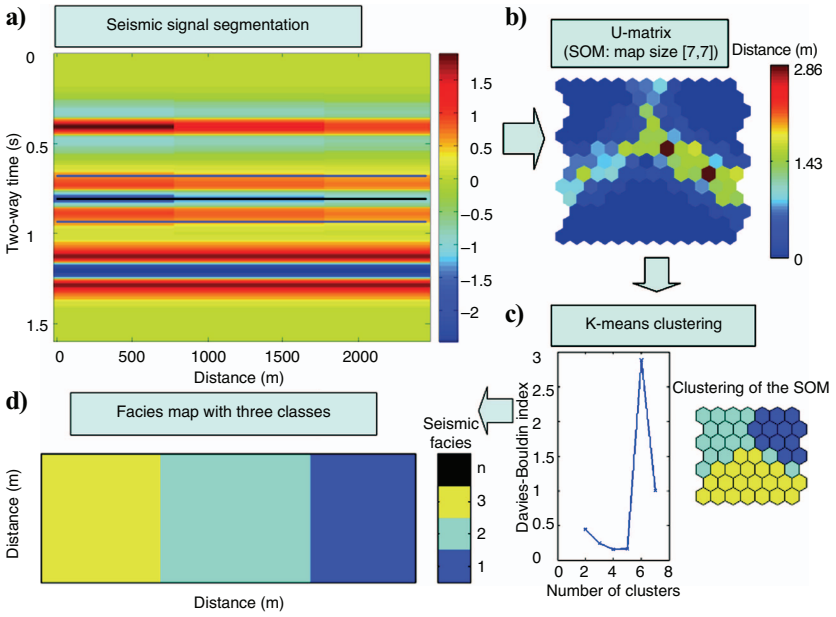

Figure 6. (a) Seismic signal temporal segmentation; color bar is amplitude; (b) U-matrix; (c) DBI; (d) seismic facies map (50×2500 m).

elastic impedance, and they can be approximated, depending on the wavefront incident angle, by the convolution of the reflectivity function with a seismic wavelet. Therefore, the waveform at the strong reflection peaks is also influenced by the geological facies variation between the stratigraphic units.

Subsurface analysis of turbidite sandstone systems shows that the reflectivity is not necessarily regular and uniform. Interpretation of waveforms in the time domain is overly sensitive to interpretation errors, which results in facies misclassifications.

Frequency-domain analysis using power-spectrum techniques has been used in seismic interpretation mainly for thin-bed detection (Partyka et al., 1999; Mafurt and Kirlin, 2001; Johann et al., 2003). However, the power spectrum does not reveal how the frequency content varies in time. On the other hand, joint time-frequency algorithms can be used to locate and to emphasize reservoir characteristics (Matos et al., 2003a, b; Castagna et al., 2003; Matos et al., 2004a, b).

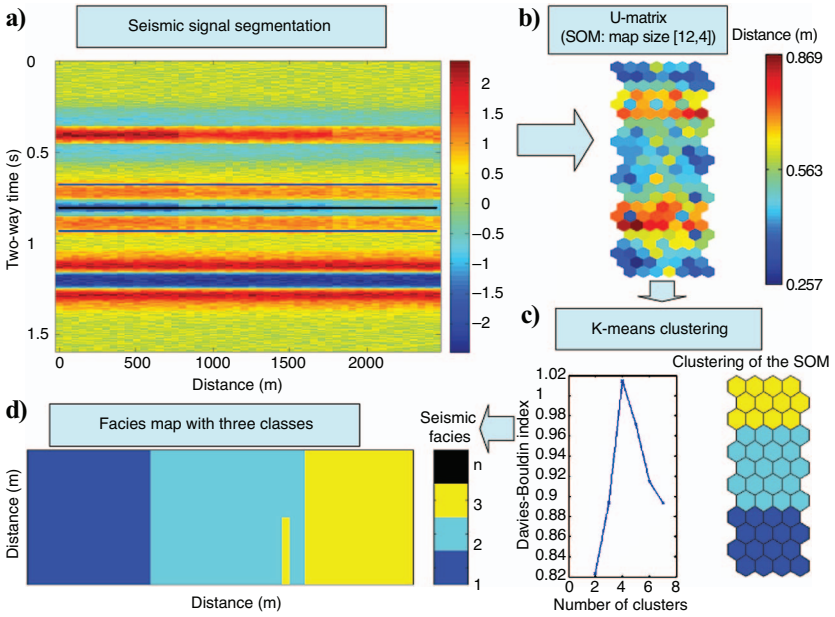

Figure 7. (a) Seismic signal temporal segmentation with Gaussian additive noise; color bar is amplitude; (b) U-matrix; (c) DBI; (d) seismic facies map (50×2500 m).

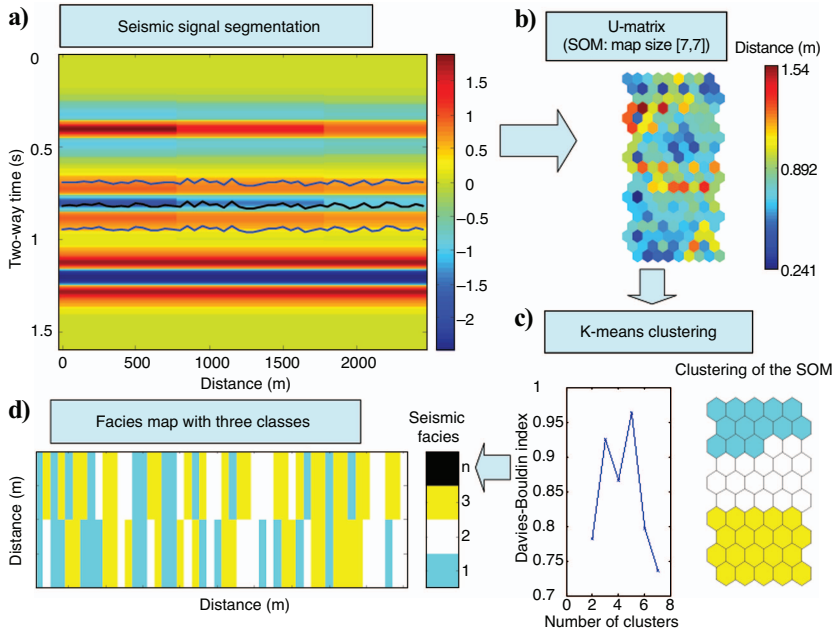

Figure 8. (a) Seismic signal temporal segmentation with interpretation error; color bar is amplitude; (b) U-matrix; color bar is distance; (c) DBI; (d) Seismic facies map; color bar represents the classes.

Continuous wavelet transform (CWT)

As formally introduced by Grossmann and Morlet (1984), a function $\psi(x) \in L^2(\Re)$ with zero mean is called a wavelet if it satisfies some well-established conditions. A family of wavelet functions can be obtained from the mother wavelet $\psi(t)$ by scaling it by s and shifting by u:

$$\psi_{u,s}(t) = \frac{1}{\sqrt{s}}\psi\left(\frac{t-u}{s}\right). \quad (7)$$

If we compress a wavelet, its spectrum will spread and move to higher frequencies. On the contrary, if we dilate a wavelet, its spectrum will compress and move to lower frequencies (Mallat, 1999). The wavelet spectrum has no DC, or zero-frequency, component.

In addition, the spectrum of each wavelet in the family maintains a constant ratio between its central frequency and the corresponding bandwidth. Once a wavelet family is chosen, then the continous wavelet transform (CWT) W of a function $f(t) \in L^2(\Re)$ at time u and scale s is defined as

$$Wf(u,s) = \frac{1}{\sqrt{s}}\int_{-\infty}^{+\infty} f(t)\psi^*\left(\frac{t-u}{s}\right)dt, \quad (8)$$

where the superscript * indicates the complex conjugate.

Because the wavelet $\psi(t)$ has zero average, the CWT can be interpreted as the crosscorrelation between the signal and the wavelet, shifted by u with scale s. Rewriting equation 8, we can also interpret the CWT as a convolution operation:

$$Wf(u,s) = \int_{-\infty}^{+\infty} f(t)\frac{1}{\sqrt{s}}\psi^*\left(\frac{t-u}{s}\right)dt$$

$$= f * \bar{\psi}_s(u), \quad (9)$$

where

$$\bar{\psi}_s(t) = \frac{1}{\sqrt{s}}\psi^*\left(-\frac{t}{s}\right). \quad (10)$$

Because the spectrum of $\psi(t)$ resembles a band-pass filter, then equation 9 can be interpreted as the convolution of the signal $f(t)$ with the band-pass filter response scaled by s.

It can be proven that the CWT preserves the signal energy and is invertible, such that, the signal can be reconstructed from the wavelet-transform coefficients (Mallat, 1999). The energy representation of the CWT coefficients is called a scalogram.

Detection and measurement of singularities through the CWT

The transitions, or irregular structures, present in any kind of signal carry information related to its physical phenomena. For instance, the image boundaries of pictures are often enough to identify and to characterize objects.

Seismic interpretation can be described as the identification of the reflectivity transitions smoothed by the seismic wavelet. Besides the horizon locations, the identified transition characterization in the interpretation is associated with geological processes. In this way, a possible transition classification could be linked to the seismic facies.

The detection of transitions or singularities in signals is based on simple mathematical concepts. The signal inflection points are associated with the first-derivative extremes, which correspond to the second-derivative zero crossings. On the basis of this concept, most of the edge detectors search to identify the transitions in multiple scales after the previous smoothing of the signal (Canny, 1986). The detection of singularities through multiple scales is related to the CWT, as described below.

Let's define a doubly differentiable smoothing function $\theta(x)$ (Jaffard et al., 2001, p. 123; Mallat and Hwang, 1992, Figure 1), with integral equal to unity, that converges to zero when x tends to $\pm\infty$. A Gaussian curve is an example of such a smoothing function. Let us define

$$\psi^a(x) = \frac{d\theta(x)}{dx}, \text{ and } \psi^b(x) = \frac{d\theta^2(x)}{dx^2}. \quad (11)$$

Because the integrals of $\psi^a(x)$ and $\psi^b(x)$ are zero in the interval $-\infty \le x \le \infty$, they can be considered to be wavelets. In this way, the CWT of a signal $f(x)$ in the scale s can be obtained by convolving the signal with a scaled wavelet. The CWTs of $f(x)$, using the two wavelets defined by equation 11, are

$$W_s^a f(x) = f * \psi_s^a(x), \quad \text{and} \quad (12)$$

$$W_s^b f(x) = f * \psi_s^b(x). \quad (13)$$

Inserting the smoothing-function derivatives into equations 12 and 13 yields

$$W_s^a f(x) = f * \left(s\frac{d\theta_s}{dx}\right)(x)$$

$$= s\frac{d}{dx}(f * \theta_s)(x), \text{ and} \quad (14)$$

$$W_s^b f(x) = f * \left(s^2\frac{d^2\theta_s}{dx^2}\right)(x)$$

$$= s^2\frac{d^2}{dx^2}(f * \theta_s)(x). \quad (15)$$

Thus, the wavelet transform $W_s^a f(x)$ and the transform $W_s^b f(x)$ are, in the scale s, the smoothed-signal first- and second-derivative, respectively. Therefore, the local extremes of $W_s^a f(x)$ relate to the zero crossings of $W_s^b f(x)$, which correspond to the inflection points of $f * \theta_s(x)$. In the case that $\theta(x)$ is a Gaussian curve, the image-boundary detection process is equivalent to the method proposed by Canny (1986).

Wavelet transform modulus maxima (WTMM)

For the signal inflection-point positions, using the CWT local peak locations, a wavelet should be chosen as the first-derivative of the smoothing function $\theta(x)$. One wavelet that fulfills this requirement is the first-derivative of the Gaussian function, called the Gauss wavelet. Figure 11b illustrates the scalogram obtained from the CWT using the Gauss wavelet for the test signal shown in Figure 11a. We can see that the scalogram local peaks coincide with the signal inflection points. Figure 11c shows the lines formed by linking these inflection points at each scale. It can be proven that these lines, which are called Wavelet Transform Modulus Maxima Lines (WTMMLs), can be used to characterize the signal irregularities through

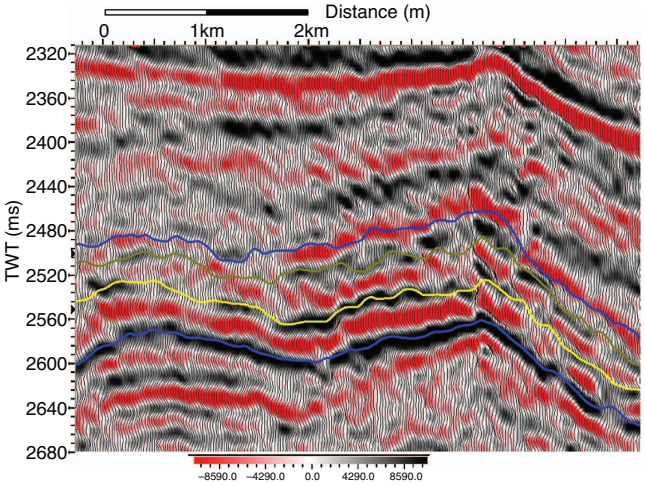

Figure 9. Seismic line extracted from the 3D real data. The blue lines represent the reservoir base and top interpretations, whereas the yellow and the green lines correspond to intermediate stratigraphic horizons. Color bar is amplitude.

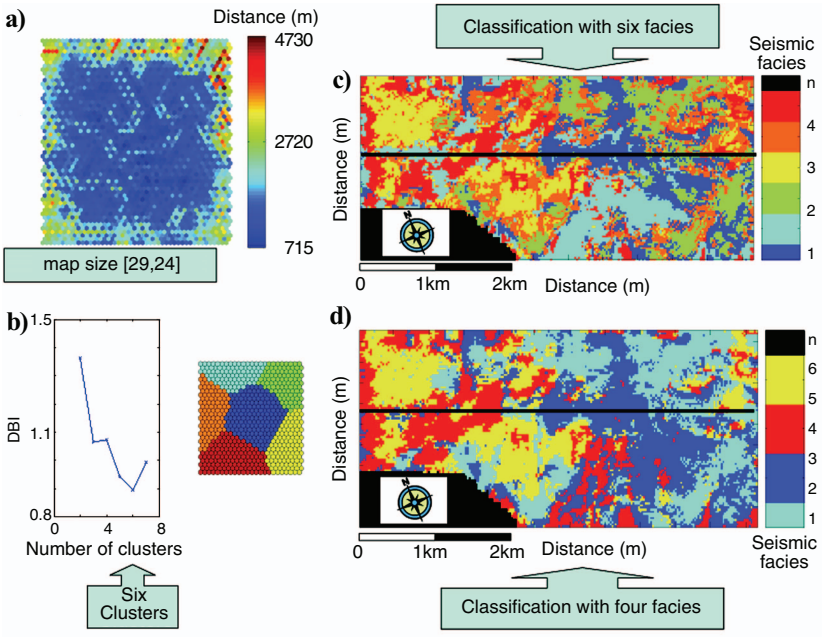

Figure 10. Real-data seismic facies analysis of the top of the reservoir; (a) U-matrix; (b) DBI; (c) seismic facies map with six facies; the black line corresponds to the seismic line location shown in Figure 9; (d) seismic facies map of the reservoir's upper stratigraphic unit with four facies; the black line corresponds to the seismic line location shown in Figure 9.

the analysis along the WTMML amplitudes, which is called Wavelet Transform Modulus Maxima Line Amplitudes (WTMMLAs) (Mallat and Hwang, 1992).

The signal irregularities can be characterized mathematically through the Lipschitz exponent (α), also called the Hölder exponent (Mallat, 1999, chap. 6). The α exponent can be obtained from the slope estimation of the curve created by the $\log_2$ of the WTMMLA coefficients divided by the $\log_2$ of the scales (Mallat, 1999, chap. 6):

$$\log_2|Wf(u,s)| \leq \log_2 A + \left(\alpha + \frac{1}{2}\right)\log_2 s. \qquad (16)$$

It should be observed that WTMML must be generated by obeying the wavelet cone of influence. The cone of influence is the area of the signal around a point at time t_0 that is taken into consideration for the CWT computation when the scale s is varied. Considering that a wavelet has a compact support in the interval $[-C_\Psi, C_\Psi]$, it is said that the CWT cone of influence along the s scales, for a certain location in the time t_0, is equal to $[t_0 - C_s, t_0 + C_s]$. Figure 12 illustrates a cone-of-influence example with respect to a location t_0.

Figure 11d illustrates the WTMMLA behavior along the scales for the discontinuity around sample 64 of the test signal shown in Figure 11a and detected by WTMML, as illustrated by Figure 11c. Figure 11e shows the Lipschitz α exponent curve corresponding to the same discontinuity. We can see in Figure 11e that the curve slope computed by the $\log_2$ of the WTMMLA is equal to 0.5. Therefore, as expected for a discontinuity, the Lipschitz exponent α is equal to zero.

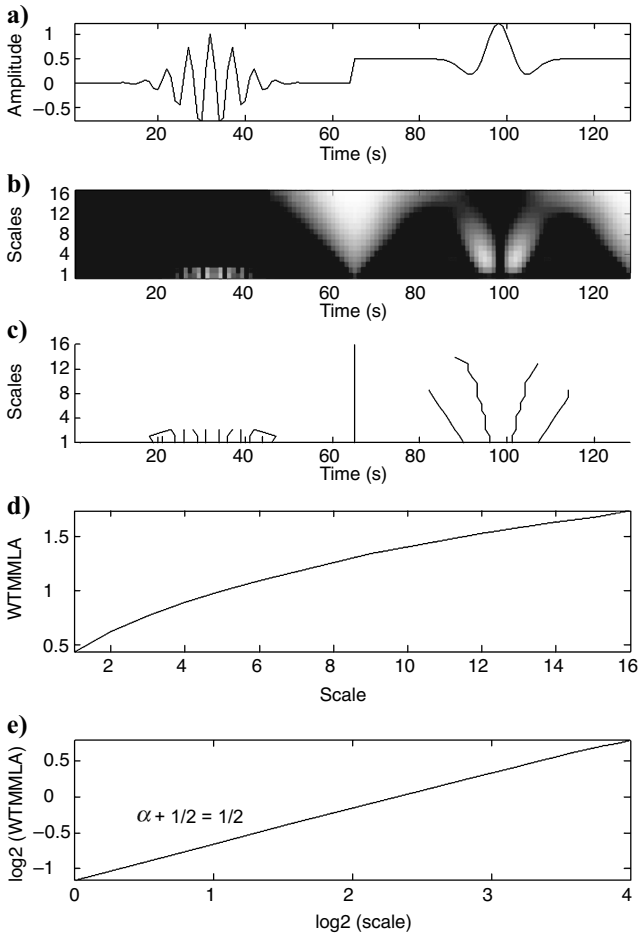

Figure 11. (a) Test signal; (b) CWT scalogram using the Gauss wavelet, in which colors close to white represent positive coefficients and colors close to black correspond to negative coefficients; (c) WTMML; (d) WTMMLA along the scales for the discontinuity detected in (a) around sample 64; (e) Lipschitz exponent obtained through WTMMLA according to equation 16.

Discrete wavelet transform without time decimation

The CWT uses families of functions created by varying continually the scale s and the displacement u parameters. This continuous variation of two parameters simultaneously results in a computationally intensive operation. In practice, this is accomplished by computing the CWT for a great number of scales.

The fastest and most common method to compute the CWT uses filter banks. In this case, it is called the Discrete Wavelet Transform (DWT) (Burrus et al., 1997). The DWT coefficients are computed in the analysis filter bank, which is a set of two filters, one half-band low pass and one half-band high pass. In the forward transform, the input signal is filtered by the two filters followed by a downsampling by a factor of two. In this context, these two last operations are called decimation. The output of the low-frequency branch is then filtered again using the same filter bank of analysis. This process continues for the number of desired levels of decomposition. This process is similar to the CWT, except for the fact that the scales change in a dyadic way, i.e., in powers of two, and owing to the decimation operations, the DWT is not invariant to displacements in time. Although efficient for data compression and some filtering operations, this last detail renders the DWT unfeasible for the detection and characterization of singularities.

An alternative way to obtain a DWT that is invariant to displacements is to remove the downsampling operation from the filter bank, which results in having only the scale as a dyadic sequence.

Mallat (1999) showed that the dyadic form makes a stable and complete representation that preserves the signal energy. Mallat and Zhong (1992) proposed a quadratic-spline wavelet family appropriate for the detection and characterization of signal singularities.

The implementation of the DWT algorithm without decimation is known as wavelet à trous (WAT), and it consists, in the signal convolution with the bank filter, of coefficients with $(2^j - 1)$ zeros inserted

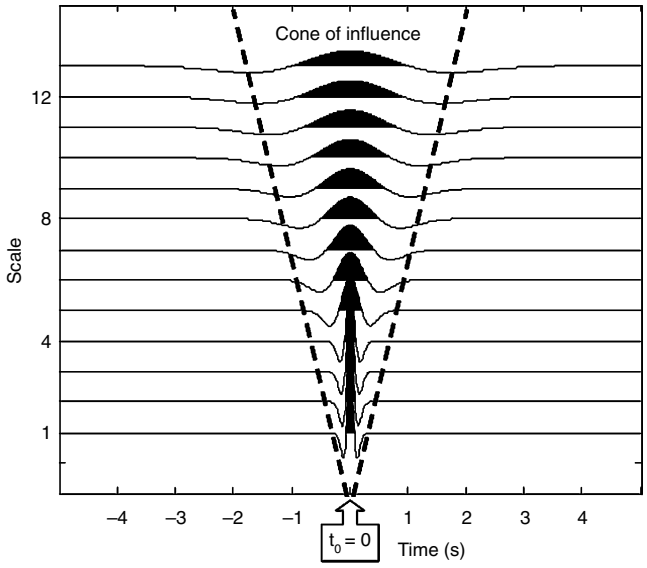

Figure 12. Wave transform cone of influence for a point located at time t_0.

between the samples (Shensa, 1992). For that reason, it is called wavelet à trous, which in French means a wavelet with holes or zeros.

We can also use the WTMM, computed through the WAT, for detection and characterization of signal singularities. Figure 13b illustrates singularity detection through WTMMLs for a test signal using only four dyadic scales, whereas Figure 13c illustrates the evolution of the WTMMLA for the singularities located around sample 100 of the test signal and detected in Figure 13a.

Hoekstra (1996) proposed to use the Lipschitz α exponent as a seismic attribute by applying the WAT to compute the WTMMLA. The Lipschitz α exponents can be computed for each WTMMLA. In the Figure 13c example, the α exponents can be estimated from four samples through a simple linear regression.

Liner et al. (2004) proposed to calculate the Hölder exponent from the CWT of a seismic trace as an instantaneous seismic attribute and called this SPICE, which became a commercial product (Li and Liner, 2004). Instead of using the WTMMLA, they proposed to estimate the slope of the curve along the scales for each localized time of the seismic trace.

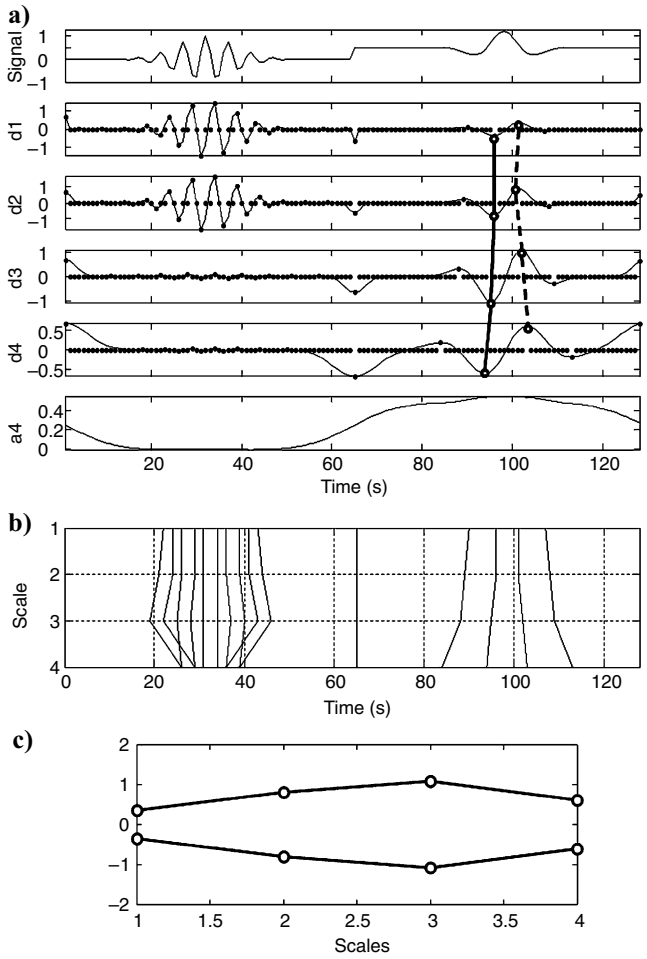

Figure 13. (a) Test signal decomposition in four levels; vertical scale is in amplitude; a4 is the approximated wavelet; (b) WTMML; (c) WTMMLA curve for the singularities located around sample 100 of the test signal detected in (a).

RESERVOIR CHARACTERIZATION USING JOINT TIME-FREQUENCY ANALYSIS PLUS SOM CLUSTERING

Principles of the methodology — Seismic facies with WT and the SOM

It can be observed that the WTMMLA curves used for the Lipschitz exponent computation can be interpreted as patterns by themselves; in other words, instead of using α as an attribute, we propose to use the whole WTMMLA curve as an input attribute for a pattern classification system. The proposed algorithm is detailed in the flowchart of Figure 14 and is shown schematically in Figure 15 (Matos et al., 2003a, b).

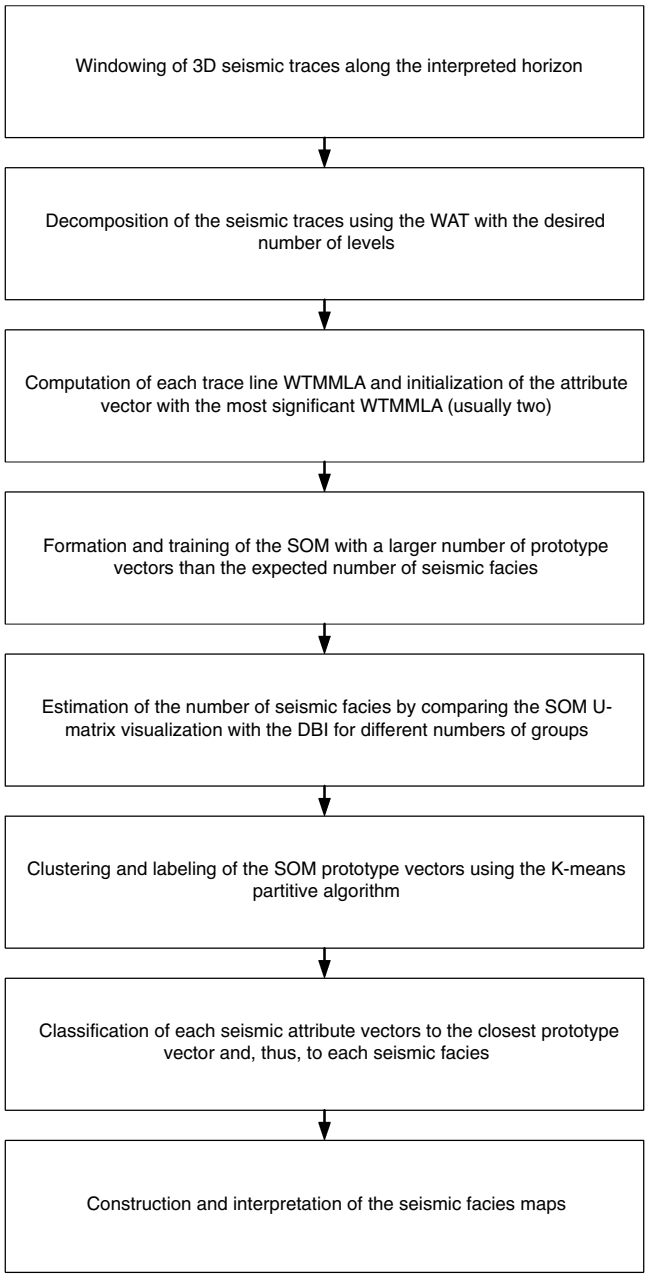

Figure 14. Workflow for nonsupervised seismic facies analysis based on SOM clustering using WTMMLA attributes (second method).

Seismic facies analysis of synthetic data — Turbidite sandstone system model

We used the same synthesized data with interpretation noise, shown in Figure 6a and repeated in Figure 16a, to test the seismic facies analysis with the second method. Figure 16d shows the resulting clusters. Comparing Figure 16c and e, we can see that the result is excellent and that it confirms the expectation about the capacity to locate seismic events in time and the consequent characterization along the scales.

Seismic facies analysis of real data — Namorado field, Campos Basin

Seismic interpretation of Namorado field reservoirs, on the basis of 45 well log data sets and 3D seismic calibration, allows the characterization of a reliable stratigraphic model with three high-resolution stratigraphic units that defined the internal architecture of these reservoirs (Johann et al., 1996; Johann, 1997). Three depositional sequences were correlated across the field, each of them corresponding to cycles of relative sea level falls.

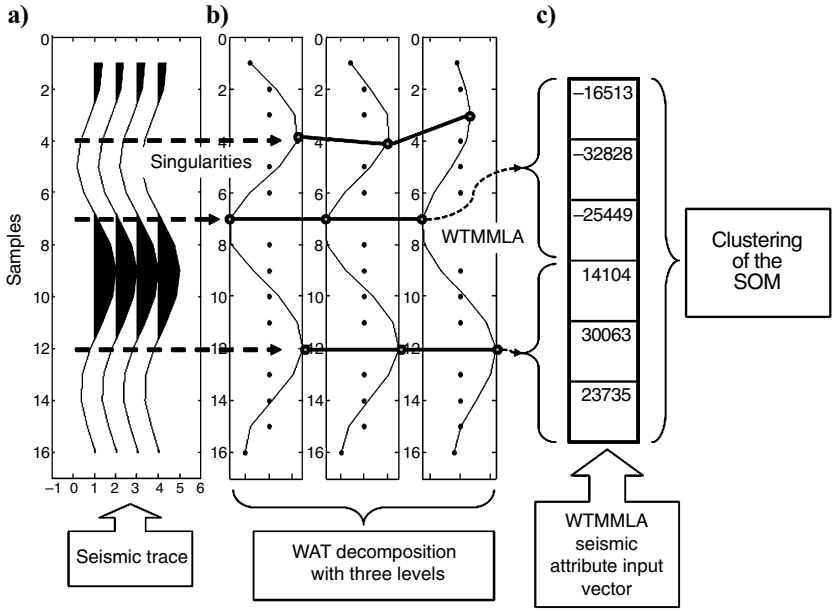

Figure 15. (a) Seismic trace from Figure 9 with 16 time samples extracted around the base horizon; the seismic trace is repeated four times; (b) WAT with three decomposition levels, d1, d2, and d3 and WTMMLA associated with the seismic trace singularities; (c) the WTMMLA seismic attribute vector example shows the two most significant WTMMLAs that maintain the time sequence. This vector is used as input to the SOM clustering algorithm.

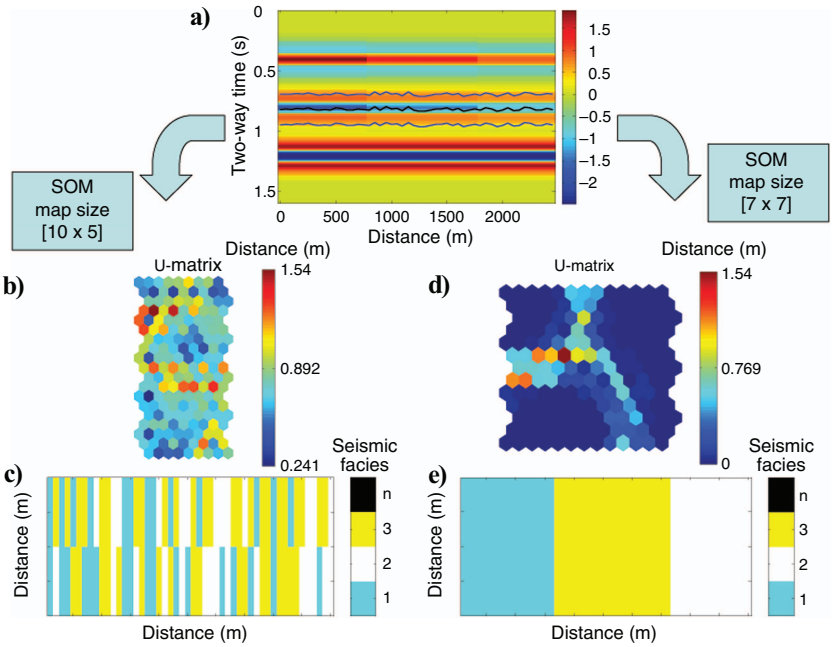

Figure 16. Seismic facies analysis of synthetic data with interpretation noise; (a) seismic data; color bar is amplitude; (b) U-matrix; (c) seismic facies map (50 × 2500 m) using the waveform as attribute; (d) U-matrix; (e) seismic facies map (50 × 2500 m) using WTMMLA attributes.

The basal unit is characterized by confined turbidite sediments deposited in the salt-controlled topographic lows (paleocanyons). The intermediate unit and the top unit are more related to classical Bouma turbidites interbeded with marls and shales (Johann, 1997).

We now apply the proposed methodology to the Campos Basin seismic data used previously. For this analysis, we used a window with 16 samples, e.g., a 64-msec time-interval window, around the horizon that delimits the top of the reservoir. The seismic facies analysis result is illustrated in Figure 17c. It can be observed in Figure 17b that the four groups formed for the analysis were well-enhanced in the U-matrix; they coincided with the facies number suggested in the petrophysics analysis and sedimentary facies analysis (Johann et al., 1996; Johann, 1997).

The seismic facies analysis was also implemented around the horizon that delimits the base of the reservoir, also taking sixteen samples. The results, illustrated in Figure 18c, are also very good; they show an interpreted paleocanyon in the Namorado field sandstone turbidite system (Figure 19). Additionally, even using an unsupervised approach, it is possible to identify an interesting petrophysics gradation that helps define the internal geometry of this high-resolution stratigraphic unit.

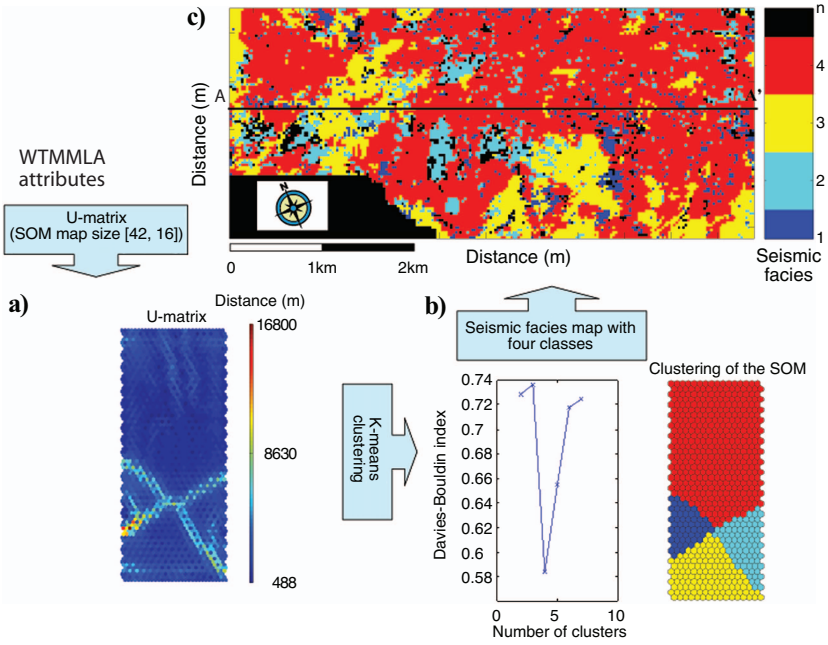

Figure 17. Real-data seismic facies analysis of the top of the reservoir using the second method; (a) U-matrix; (b) DBI; (c) seismic facies map; the black line corresponds to the seismic line location shown in Figure 9.

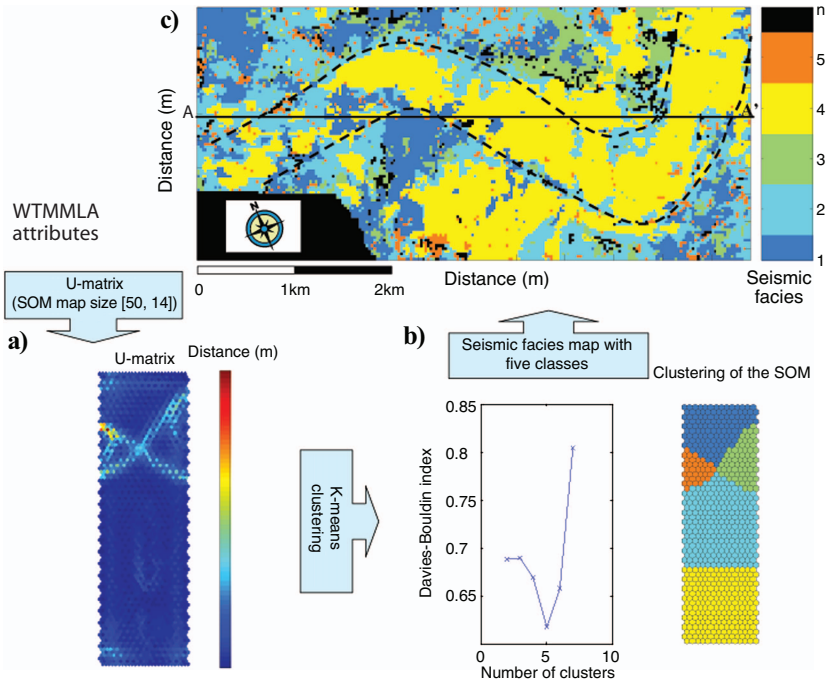

Figure 18. Real-data seismic facies analysis of the base of the reservoir using the second method; (a) U-matrix; (b) DBI; (c) seismic facies map; the black line corresponds to the seismic line location shown in Figure 9; the dotted black lines correspond to the basal paleocanyon.

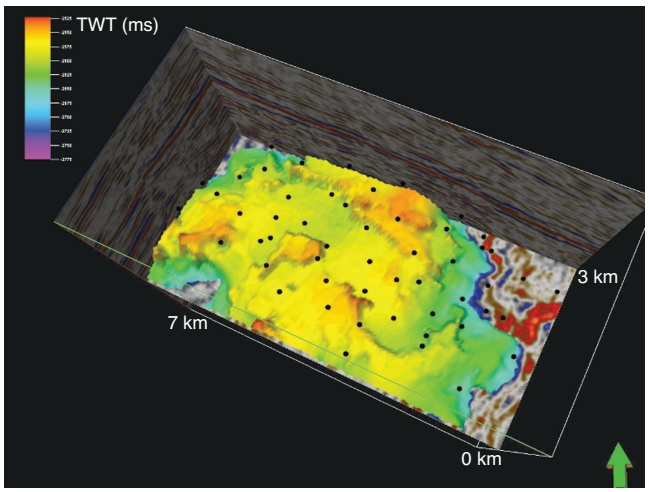

Figure 19. 3D view of structural time map of the Namorado field reservoir basal turbidite sandstone system.

The excellent result of the seismic facies analysis, using WTMMLA for synthetic data, and the coherent results obtained for realdata suggest that the second method proposed in this work is an important tool for reservoir characterization as well as for seismic exploration, mainly, because it is less sensitive to interpretation errors.

CONCLUSIONS

In this paper we proposed two methods to estimate, in a semiautomatic way, the number of seismic facies and also to create seismic facies maps. The first method estimates the number of facies from the U-matrix visualization and the DBI, computed from the SOM clustering. The main drawback of this method is its sensitivity to interpretation errors, especially when seismic-trace amplitudes are the input data to the algorithm.

In the second method, we employed time-frequency techniques that use the WAT as a preprocessing tool to a pattern classification system, which also uses the SOM clustering. The use of WAT to locate events in time through the identification of signal singularities also proved to be useful as an appropriate tool for detection of seismic events. Because the evolution of the WTMMLA characterizes the signal singularities, we used it as a seismic attribute vector related to the detected events. This approach has clear advantages over other techniques that use, for instance, the Lipschit coefficient as a seismic attribute. The SOM integration, as a classification tool associated with the patterns generated using the WAT, has proven to be an effective tool in 3D seismic reservoir characterization. The second method also proved to be less sensitive to interpretation errors.

It should be emphasized that the objective of this work was not to obtain an optimal way to cluster the data but, instead, to identify and to separate different characteristics in large data sets, as is the case of seismic data. Obviously, this approach is only valid when the identified groups, using the SOM, are similar to those of the original data.

The results obtained with 3D seismic data suggest that the second method can also be used for 4D analyses, which is currently being investigated. Such a statement is based on the fact that the anomalies already explored in a certain area would probably have their associated singularities altered because of the changes in the reservoir properties related to the oil and/or gas production.

ACKNOWLEDGMENTS

The authors thank ANP (Brazilian Petroleum Agency) and Petrobras for permission to use the seismic data contained herein and acknowledge Petrobras financial support through the Petrobras Strategic Research Program in Reservoir Geophysics, PRAVAP 19. The authors are grateful to GEOPHYSICS associate editor Kurt Marfurt for his patience in providing a thorough review of the manuscript, which greatly improved its quality. Thanks to the reviewers for their constructive comments.

LIST OF SYMBOLS

α = Lipschit or Hölder exponent
K = number of SOM groups
c_k = group k centroid in the K-means partitive clustering
d_{kl} = distance between group centroids in the K-means partitive clustering
$\theta(x)$ = smoothing function in the time-frequency method
D = number of SOM map elements
$h_{bi}(t)$ = neighborhood size entered at the winner unit in the SOM algorithm
$\lambda(t)$ = learning rate in the SOM algorithm
$\boldsymbol{m}_i$ = prototype vectors $i = 1,2,\ldots,P$ in the SOM algorithm
$\boldsymbol{m}_b$ = smallest distance to the input vector x in the SOM algorithm
n = number of input seismic attributes
P = number of prototype vectors in the SOM algorithm
S_k = average distance between each element and its group centroid in the K-means partitive clustering
$\psi(t)$ = mother wavelet
$\psi^a(x)$ = first derivative of $\theta(x)$
$\psi^b(x)$ = second derivative of $\theta(x)$
r_b = position of the prototype vector $\boldsymbol{b}$ in the SOM grid
r_i = position of the prototype vector $\boldsymbol{i}$ in the SOM grid
s = continuous wavelet scale coefficient
u = continuous wavelet translation coefficient
x = input vector of dimension n in the SOM algorithm
$W_{u,s}(t)$ = family of continuous wavelet functions

REFERENCES

Burrus, C. S., H. Guo, and R. A. Gopinath, 1997, Introduction to wavelets and wavelet transforms: A primer: Prentice-Hall, Inc.
Canny, J., 1986, A computational approach to edge detection: IEEE Transactions on Pattern Analysis and Machine Intelligence, **36**, 961–1005.
Castagna, J. P., S. Sun, and R. W. Siegfried, 2003, Instantaneous spectral analysis: Detection of low-frequency shadows associated with hydrocarbons: The Leading Edge, **22**, 120–127.
Coléou, T., M. Poupon, and K. Azbel, 2003, Interpreter's Corner — Unsupervised seismic facies classification: A review and comparison of techniques and implementation: The Leading Edge, **22**, 942–953.
Costa, J. A. F., and M. L. A. Netto, 1999, Cluster analysis using self-organiz-

ing maps and image processing techniques: IEEE International Conference on Systems, Man, and Cybernetics, **5**, 367–372.
Davies, D. L., and D. W. Bouldin, 1979, A cluster separation measure: IEEE Transactions on Pattern Analysis and Machine Intelligence, **PAMI-1**, 2 224–227.
Duda, R. O., P. O. Hart, and D. G. Stork, 2001, Pattern classification, 2nd ed.: John Wiley & Sons, Inc.
Dumay, J., and F. Fournier, 1988, Multivariate statistical analyses applied to seismic facies recognition: Geophysics, **53**, 1151–1159.
Fournier, F., and J. F. Derain, 1995, A statistical methodology for deriving reservoir properties from seismic data: Geophysics, **60**, 1437–1450.
Grossmann, A., and J. Morlet, 1984, Decomposition of Hardy functions into square integrable wavelets of constant shape: SIAM Journal on Mathematical Analysis, **15**, 723–736.
Haykin, S., 1999, Neural networks: A comprehensive foundation, 2nd ed.: Prentice Hall.
Hoekstra, E. V., 1996, Multiscale analysis of seismic data by the wavelet transform: M.S. thesis, Delft University of Technology.
Jaffard, S., R. D. Ryan, and Y. Meyer, 2001, Wavelets: Tools for science & technology, 1st ed.: SIAM.
Johann, P. R. S., 1997, Inversion sismo-stratigraphique et simulations stochastiques: Reservoir turbiditique, offshore du Brésil. Intégration géologique, géophysique et géostatistique en 3-D: Ph.D. thesis, Université de Paris VI.
Johann, P. R. S., D. D. Castro, and A. S. Barroso, 2001, Reservoir geophysics: Seismic pattern recognition applied to ultra-deepwater oilfield in Campos basin, offshore Brazil: SPE Latin America and Caribbean Petroleum Engineering Conference.
Johann, P. R. S., F. Fournier, P. Dequirez, Jr., and C. Blanchet, 1996, 3-D reservoir characterization by stratigraphic inversion and pattern recognition: 66th Annual International Meeting, SEG, Expanded Abstracts, **15**, 1797–1800.
Johann, P. R. S., G. Ragagnin, and M. Spínola, 2003, Spectral decomposition reveals geological hidden features in the amplitude maps from a deep water reservoir in the Campos basin: 73rd Annual International Meeting, SEG, Expanded Abstracts, 1740–1743.
Kohonen, T., 2001, Self-organizing maps, 3rd ed.: Springer-Verlag.
Li, C. F., and C. L. Liner, 2004, Wavelet-based analysis of singularities in seismic data: United States Patent: US 6 745 129 B1.
Liner, C., C. F. Li, A. Gersztenkorn, and J. Smythe, 2004, SPICE: A new general seismic attribute: 74th Annual International Meeting, SEG, Expanded Abstracts, 433–436.
Mallat, S., 1999, A wavelet tour of signal processing: Academic Press Inc.
Mallat, S., and W. L. Hwang, 1992, Singularity detection and processing with wavelets: IEEE Transactions on Information Theory, **38**, 617–643.
Mallat, S., and S. Zhong, 1992, Characterization of signals from multiscale edges: IEEE Transactions on Pattern Analysis and Machine Intelligence, **14**, 710–732.
Marfurt, K. J., and R. L. Kirlin, 2001, Narrow-band spectral analysis and thin-bed tuning: Geophysics, **66**, 1274–1283.
Matos, M. C., P. L. M. Osorio, and P. R. S. Johann, 2003a, Using wavelet transform and self-organizing maps for seismic reservoir characterization of a deep-water field, Campos basin, offshore Brazil: 65th Annual Conference and Exhibition, EAGE, Extended Abstracts, B29.
——–, 2003b, Unsupervised seismic reservoir characterization using wavelet transform and self-organizing maps of a deep-water field, Campos basin, offshore Brazil: 73rd Annual International Meeting, SEG, Expanded Abstracts, 1458–1461.
——–, 2004a, Unsupervised seismic facies classification using matching pursuit and self organizing maps: 66th Annual Conference and Exhibition, EAGE.
——–, 2004b, Using matching pursuit and self organizing maps for seismic reservoir characterization of a deep-water field, Campos basin, offshore Brazil: 74th Annual International Meeting, SEG, Expanded Abstracts, 1611–1614.
Mitchum, R. M., 1977, Glossary of terms used in seismic stratigraphy: AAPG Memoir 26, 205–212.
Pandya, A. S., and R. S. Macy, 1995, Pattern recognition with neural networks in C++: CRC Press.
Partyka, G., J. Gridley, and J. Lopez, 1999, Interpretational applications of spectral decomposition in reservoir characterization: The Leading Edge, **18**, 353–360.
Poupon, M., J. Gil, D. Vannaxay, and B. Cortiula, 2004, Tracking delta sands: A seismic facies classification and 3D visualization workflow (Urdaneta West, Lake Maracaibo-Venezuela): The Leading Edge, **23**, 909–912.
Rankey, E. C., and J. C. Mitchell, 2003, Interpreter's Corner — That's why it's called interpretation: Impact of horizon uncertainty on seismic attribute analysis: The Leading Edge, **22**, 820–828.
Saggaf, M. M., M. N. Toksöz, and M. I. Marhoon, 2003, Seismic facies classification and identification by competitive neural networks: Geophysics, **68**, 1984–1999.
Santos, M. S., 1997, Caracterização de reservatórios via redes neurais: M.Sc. thesis, Bahia Federal University.
Schultz, P., S. Ronen, M. Hattori, and C. Corbert, 1994, Seismic-guided estimation of log properties, Part 2: Using artificial neural networks for nonlinear attribute calibration: The Leading Edge, **13**, 674–678.
Shensa, M. J., 1992, The discrete wavelet transform: Wedding the à trous and Mallat algorithms: IEEE Transactions on Signal Processing, **40**, 2464–2482.
Sheriff, R. E., 2002, Encyclopedic dictionary of applied geophysics, 4th ed.: SEG.
Steeghs, P., and G. Drijkoningen, 2001, Seismic sequence analysis and attribute extraction using quadratic time-frequency representations: Geophysics, **66**, 1947–1959.
Taner, M. T., J. S. Schuelke, R. O'Doherty, and E. Baysal, 1994, Seismic attributes revisited: 64th Annual International Meeting, SEG, Expanded Abstracts, **13**, 1104.
Taner, M. T., J. D. Walls, M. Smith, G. Taylor, M. B. Carr, and D. Dumas, 2001, Reservoir characterization by calibration of self-organized map clusters: 71st Annual International Meeting, SEG, Expanded Abstracts, **20**, 1522–1525.
Theodoridis, S., and K. Koutroumbras, 1999, Pattern Recognition: Academic Press Inc.
Ultsch, A., 1993, Knowledge extraction from self-organizing neural networks, *in* Opitz et al., eds., Information and classification: Springer-Verlag.
Vesanto, J., and E. Alhoniemi, 2000, Clustering of the self-organizing map: IEEE Transactions on Neural Networks, **11**, 586–600.
Vesanto, J., J. Himberg, E. Alhoniemi, and J. Parhankangas, 1999, Self-organizing map in Matlab: The SOM toolbox: Proceedings of the Matlab DSP Conference.
Walls, J. D., M. T. Taner, T. Guidish, G. Taylor, D. Dumas, and N. Derzhi, 1999, North Sea reservoir characterization using rock physics, seismic attributes, and neural networks; A case history: 69th Annual International Meeting, SEG, Expanded Abstracts, **18**, 1572.
Zhang, L., J. Quieren, and J. Schuelke, 2001, Self-organizing map (SOM) network for tracking horizons and classifying seismic traces, *in* M. Poulton, ed., Computational neural networks for geophysical data: Pergamon Press, Inc.